

# XMM-NEWTON OBSERVATIONS OF THE BIPOLAR PLANETARY NEBULAE NGC 2346 AND NGC 7026

ROBERT A. GRUENDL<sup>1</sup>, MARTÍN A. GUERRERO<sup>2</sup>, YOU-HUA CHU<sup>1</sup>, AND ROSA M. WILLIAMS<sup>1</sup>

*Draft version August 10, 2018*

## ABSTRACT

We have obtained X-ray observations of the bipolar planetary nebulae (PNe) NGC 2346 and NGC 7026 with *XMM-Newton*. These observations detected diffuse X-ray emission from NGC 7026 but not from NGC 2346. The X-ray emission from NGC 7026 appears to be confined within the bipolar lobes of the PN and has spectral properties suggesting a thermal plasma emitting at a temperature of  $1.1_{-0.2}^{+0.5} \times 10^6$  K. The X-ray spectrum of NGC 7026 is modeled using nebular and stellar abundances to assess whether a significant amount of nebular material has been mixed into the shocked-wind, but the results of this comparison are not conclusive owing to the small number of counts detected. Observations of bipolar PNe indicate that diffuse X-ray emission is much less likely detected in open-lobed nebulae than closed-lobed nebulae, possibly because open-lobed nebulae do not have strong fast winds or are unable to retain hot gas.

*Subject headings:* planetary nebulae: general — planetary nebulae: individual (NGC 2346, NGC 7026)  
— X-rays: ISM — stars: winds

## 1. INTRODUCTION

Planetary nebulae (PNe) consist of the stellar mass lost by their low- or intermediate-mass stellar progenitors during late evolutionary stages. As a star evolves past the asymptotic giant branch (AGB) phase, the mass loss process changes from a copious slow AGB wind to a tenuous fast wind and the interaction between the fast wind and the AGB wind forms a PN (Kwok 1983). Frank & Mellema (1994) have demonstrated that this wind-wind interaction can produce the commonly observed elliptical and bipolar morphologies of PNe, although the bipolar morphology requires that either the AGB wind or the fast stellar wind is anisotropic and has a polar angle dependence.

The geometry of the fast wind has often been assumed to be isotropic, but the presence of bipolar jets and collimated outflows in some PNe indicates that the fast wind may span a range of geometries. For wind velocities greater than  $\sim 300$  km s<sup>-1</sup>, the interaction of the fast stellar wind with the AGB wind will shock-heat the wind material to temperatures greater than  $10^6$  K. This shocked fast stellar wind is too tenuous to produce appreciable X-ray emission, but at its interface with the dense nebular material, heat conduction lowers the temperature and mass evaporation raises the density of the shocked fast wind, producing optimal conditions for X-ray emission (Weaver et al. 1977; Zhekov & Perinotto 1996). Since the hot gas in a PN is associated with shocked fast wind, the distribution of X-ray emission may be used to infer a directional dependence for the fast wind.

*Chandra* and *XMM-Newton* observations of elliptical PNe have revealed diffuse X-ray emission confined within their innermost nebular shells, e.g., NGC 2392 (Guerrero et al. 2005a) and NGC 6543 (Chu et al. 2001).

The plasma temperatures implied by their X-ray spectra are a few times  $10^6$  K. In the case of NGC 6543, the X-ray emission is well resolved, and a clear limb-brightening is observed. Of the ten elliptical PNe observed by either *XMM-Newton* or *Chandra*, six show detectable diffuse X-ray emission (Guerrero et al. 2005b).

*Chandra* has observed many bipolar PNe. While two of them, Mz 3 and NGC 7027, exhibit diffuse X-ray emission confined within the bipolar lobes (Kastner et al. 2001, 2003), the other bipolar PNe (e.g., MyCn 18, M 1-16, M 1-92, M 2-9, OH 231.8+4.2) were not detected. Most of these non-detections are understandable because they are associated with relatively young/exotic bipolar PNe that either have large circumstellar absorption or have collimated outflows with low wind/outflow velocities,  $< 300$  km s<sup>-1</sup>. In order to better characterize diffuse X-ray emission from bipolar PNe, we have used *XMM-Newton* to observe two carefully chosen bipolar PNe with contrasting lobe morphologies, NGC 2346 and NGC 7026.

NGC 2346 has a butterfly morphology with two open bipolar lobes and a bright equatorial waist that contains large amounts of molecular gas and dust (Walsh et al. 1991; Zuckerman & Gatley 1988; Su et al. 2004). Its central star is a white dwarf with an A5 companion (Méndez 1978), forming a single-line spectroscopic binary with a period of  $\sim 16$  days (Méndez & Niemela 1981). Its nebular gas shows a bipolar velocity field with a dynamic age of 3,500–4,700 yrs (Walsh et al. 1991; Arias et al. 2001). NGC 2346 can be described as an evolved bipolar PN.

NGC 7026 has closed bipolar lobes emanating from a bright ring-like waist (Solf & Weinberger 1984), and the lobes appear to have multiple components (Cuesta, Phillips, & Mampaso 1996; López 2003). Its central star is a hydrogen-deficient WC star (Aller 1976; Acker & Neiner 2003). The dynamic age derived from the nebular expansion,  $< 1,000$  yrs, suggests that NGC 7026 is a young bipolar PN (Solf & Weinberger 1984).

The *XMM-Newton* observations of these two PNe have detected diffuse X-ray emission from NGC 7026, but not

arXiv:astro-ph/0607519v1 22 Jul 2006

<sup>1</sup> Astronomy Department, University of Illinois, 1002 W. Green Street, Urbana, IL 61801, USA; gruendl@astro.uiuc.edu, chu@astro.uiuc.edu, rosanina@astro.uiuc.edu

<sup>2</sup> Instituto de Astrofísica de Andalucía, Consejo Superior de Investigaciones Científicas (CSIC), Apartado Correos 3004, E-18080, Granada, Spain; mar@iaa.es

from NGC 2346. In this paper, we describe these X-ray observations and their reduction in §2, report our analysis of the observations in §3, and discuss their implications in §4.

## 2. OBSERVATIONS

NGC 2346 and NGC 7026 were observed with *XMM-Newton* in Revolution 876 (Obs ID 0200240501) on 2004 September 20 and Revolution 825 (Obs ID 0200240101) on 2004 June 10, respectively. The European Photon Imaging Camera (EPIC), which consists of two MOS and one PN CCD arrays, was used with a medium filter. The two EPIC/MOS cameras were operated in the Full-Frame Mode for a total exposure time of 16.5 ks for NGC 2346 and 19.2 ks for NGC 7026. The EPIC/pn camera was operated in the Extended Full-Frame Mode for a total exposure time of 11.1 ks for NGC 2346 and 14.1 ks for NGC 7026.

The *XMM-Newton* pipeline products have been processed using the *XMM-Newton* Science Analysis Software (SAS version 6.1.0) and the calibration files from the Calibration Access Layer available on 2005 April 22. The event files have been screened to eliminate bad events and periods of high background. For the EPIC/MOS observations, only events with CCD patterns 0–12 (similar to *ASCA* grades 0–4) were selected; for the EPIC/pn observation, only events with CCD pattern 0 (single pixel events) were selected. To assess the background rate, we obtained light curves for each instrument in the 10–12 keV energy range, where the counts are dominated by the background. The time intervals with high background, i.e., count rates  $\geq 0.25$  cts  $s^{-1}$  for the EPIC/MOS or  $\geq 1.0$  cts  $s^{-1}$  for the EPIC/pn, were discarded. The resulting exposure times for the EPIC/MOS and EPIC/pn observations were 16.5 ks and 10.9 ks for NGC 2346 and 15.5 ks and 13.3 ks for NGC 7026, respectively.

## 3. RESULTS

X-ray emission was clearly detected from NGC 7026 but not from NGC 2346. We therefore describe the results from NGC 7026 first and then determine an upper limit for the X-ray luminosity of NGC 2346.

### 3.1. NGC 7026: Spatial Properties

To measure the faint X-ray emission from NGC 7026, we used a  $60'' \times 40''$  elliptical source aperture that encompasses the entire optical nebula and a background aperture  $\sim 5$  times as large as the source aperture located at a similar Y-coordinate of the detector. The EPIC/pn observation detected a total of  $110 \pm 15$  background-subtracted counts, corresponding to a count rate of  $8.3 \times 10^{-3}$  cts  $s^{-1}$ . The EPIC/MOS1 and EPIC/MOS2 observations detected  $26 \pm 8$  and  $31 \pm 8$  background-subtracted counts, corresponding to count rates of  $1.7 \times 10^{-3}$  cts  $s^{-1}$  and  $2.0 \times 10^{-3}$  cts  $s^{-1}$ , respectively.

We have merged the EPIC/pn and EPIC/MOS images to increase the signal-to-noise ratio. The merged EPIC image is displayed in Figure 1a and a smoothed image in Figure 1b. Diffuse X-ray emission is clearly detected. In order to compare the distribution of X-ray emission with the optical nebula, accurate alignment between X-ray and optical images is essential. We have determined

the astrometric solution for the EPIC image with an accuracy of  $\sim 0''.5$ , based on stellar sources that are detected in both this X-ray image and the *Digitized Sky Survey*. The relative alignment of the EPIC image and a Nordic Optical Telescope (NOT) [N II] image in Figure 1c is accurate to  $\sim 0''.6$ .

The distribution of diffuse X-ray emission from NGC 7026 is elongated in the North-South direction, matching the polar axis of the nebula. The position and orientation of the 50% contour of the smoothed EPIC image follow the bipolar lobes shown in the NOT [N II] image (Fig. 1c). Furthermore, the X-ray emission shows two peaks that are projected within the bipolar lobes north and south of the central waist of NGC 7026. These excellent correspondences suggest that the diffuse X-ray emission from NGC 7026 is all confined within its bipolar lobes, similar to what is seen in the bipolar PN Mz 3 (Kastner et al. 2003).

We have simulated the surface brightness of diffuse X-ray emission assuming the hot gas is distributed in two spherical shells with fractional shell thickness ( $\Delta R/R$ ) of 0.1, 0.2, 0.5, and 1.0. We find that the small number of counts and limited angular resolution precludes even a rough estimate of the geometry. Similarly, we cannot determine whether the local minimum along the waist is caused by higher circumstellar absorption.

### 3.2. NGC 7026: Spectral Properties

X-ray spectra of NGC 7026 have been extracted from the event files of the three *XMM-Newton* EPIC cameras using the same source and background apertures described in §3.1. Due to the limited number of counts detected by the EPIC/MOS observations, we will limit the spectral analysis to the EPIC/pn spectrum shown in Figure 2. This spectrum is soft, peaking at  $\sim 0.5$  keV with a nearly flat distribution from 0.2 to 0.4 keV. Emission between 0.7 and 1.1 keV is detected but with low S/N ratio. There is no detectable emission at energies greater than 1.25 keV.

The EPIC/pn spectrum of NGC 7026, similar to other PNe, is suggestive of thermal plasma emission with its broad peak at  $\sim 0.5$  keV corresponding to emission from the He-like triplets of N VI at  $\sim 0.43$  keV and O VII at  $\sim 0.57$  keV. In order to model this X-ray spectrum, we have adopted the MEKAL thin plasma emission model (Kaastra & Mewe 1993; Liedahl, Osterheld, & Goldstein 1995). Spectral fits were carried out by folding the thin plasma emission model spectrum through the EPIC/pn response matrix, and comparing the modeled spectrum to the observed EPIC/pn spectrum in the 0.25–1.5 keV energy range after the spectrum was resampled to energy bins with at least 16 counts. The best-fit was judged based on the  $\chi^2$  statistics. It was found that the spectral fits did not accurately constrain the absorption column density,  $N_H$ , if it was allowed to vary as a free parameter. We therefore held  $N_H$  fixed at  $3.2 \times 10^{21}$   $cm^{-2}$ , estimated from the observed logarithmic extinction in the H $\beta$  line  $c(H\beta) = 0.8 \pm 0.1$  (Kwitter & Henry 2001; Hyung & Feibelman 2004) and the canonical gas-to-dust ratio of  $N_H/E(B-V) = 5.8 \times 10^{21}$  atoms  $cm^{-2}$  mag $^{-1}$  (Bohlin, Savage & Drake 1978). The X-ray-emitting gas consists of shocked fast wind and mixed-in nebular gas. As the wind abundances determined from UV spectroscopic observations

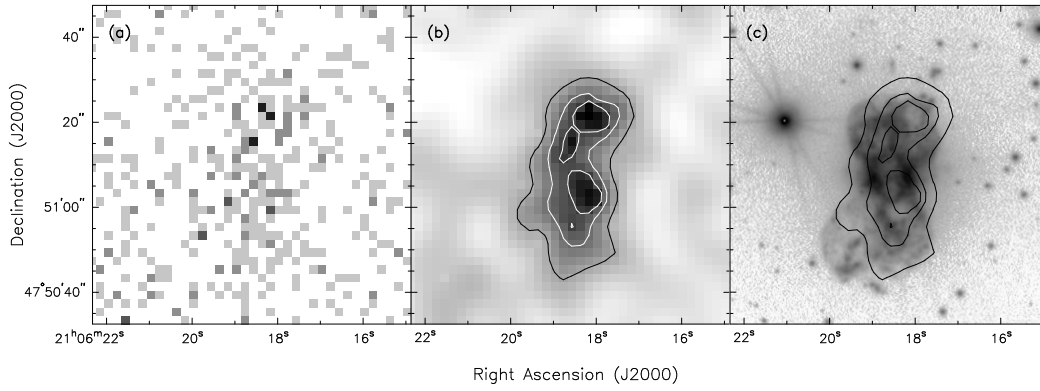


FIG. 1.— *XMM-Newton* and NOT [N II] images of NGC 7026. Panel (a) displays the *XMM-Newton* EPIC raw image in the 0.4-1.1 keV band with pixel size  $2''.0$ . This energy band includes most of the photons detected from NGC 7026 as illustrated by its EPIC/pn X-ray spectrum shown in Fig. 2. Panel (b) shows a grey-scale presentation of an adaptively smoothed EPIC image using Gaussian profiles with FWHM ranging from  $1''.5$  to  $4''$ . The X-ray contours overplotted correspond to 50%, 75%, and 95% of the peak level. Panel (c) displays the NOT [N II] image overplotted by these same X-ray contours. Panel (d) shows a color-composite image comprised of the smoothed *XMM-Newton* EPIC image (blue) and *HST* images obtained with the F502N (green) and F658N (red) filters to show [O III] and [N II] emission.

(Koesterke 2001; Hamann, Todt & Graefener 2005) differ from the nebular abundances determined from optical spectra (Kwitter & Henry 2001), we have made spectral fits using wind or nebular abundances separately.

The first spectral fits use the nebular abundances, with the number ratio of He, O, N, Ne, Ar, Cl,

and S to hydrogen being  $0.14$ ,  $7.3 \times 10^{-4}$ ,  $5.5 \times 10^{-4}$ ,  $1.8 \times 10^{-4}$ ,  $3.1 \times 10^{-6}$ ,  $3.7 \times 10^{-7}$ , and  $1.4 \times 10^{-5}$ , respectively (Kwitter & Henry 2001). The corresponding nebular abundances of these elements relative to the solar values (Anders & Grevesse 1989) are 1.43, 0.86, 4.9, 1.8, 1.5, 2.0, and 0.96, respectively. Solar abun-

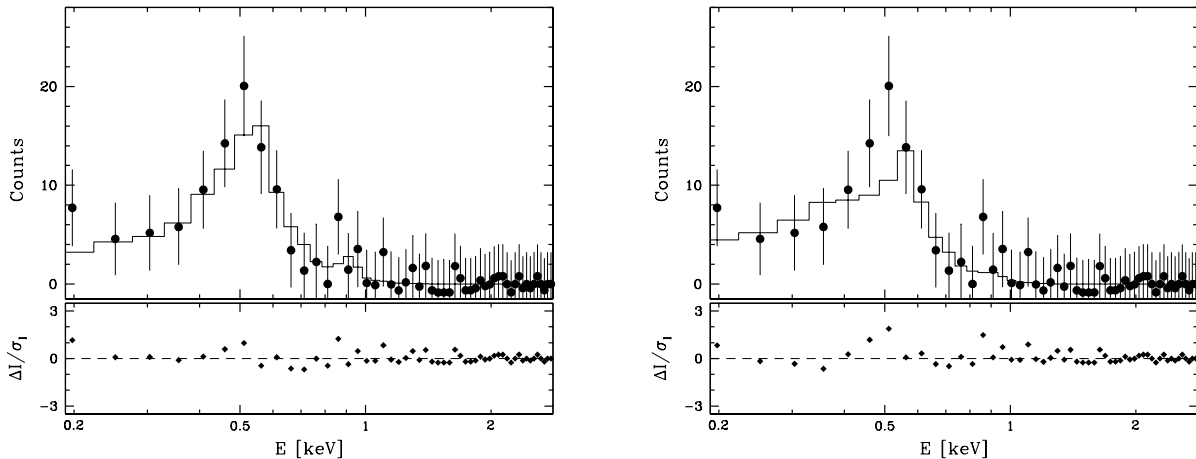


FIG. 2.— (left) *XMM-Newton* EPIC/pn background-subtracted spectrum of NGC 7026 overplotted with the best-fit MEKAL model assuming nebular abundances (solid line). (right) the same spectrum overplotted with the best-fit MEKAL model assuming the abundances of the central star. For plotting purposes, both the spectrum and model are binned in 50 eV wide energy bins to preserve the EPIC/pn spectral resolution of  $\sim 100$  eV at 1 keV. Beneath each spectrum the residuals from the best-fit are plotted.

dances are used for the other elements, which have low abundances and are not expected to contribute significantly to the diffuse X-ray emission. We have also assumed solar abundances for the foreground interstellar absorption, and adopted absorption cross-sections from Balucinska-Church & McCammon (1992). The resulting best-fit model with nebular abundances and a fixed  $N_{\text{H}}$  is overplotted on the EPIC/pn spectrum in Figure 2a. The plasma temperature of the best-fit model is  $T = (1.1^{+0.5}_{-0.2}) \times 10^6$  K (i.e.,  $kT = 0.095^{+0.045}_{-0.015}$  keV).

The second spectral fits use stellar abundances. The central star of NGC 7026 has been classified as a hydrogen-deficient WC star with the mass-fractions of He, C, and O being 70, 20, and 10%, respectively (Koesterke 2001; Hamann et al. 2005). In order to make spectral fits using a MEKAL model we have assumed a He/H ratio of 200 and scaled the abundances of C and O according to their mass fractions. Thus, the values adopted for the stellar wind abundances relative to the solar values were 20, 500, and 80 for He, C, and O, respectively. All other abundances were set to zero and the absorption column density,  $N_{\text{H}}$ , was again held fixed with a value of  $3.2 \times 10^{21}$  cm $^{-2}$ . The resulting best-fit model is shown in Figure 2b. This model with stellar abundances has roughly the same temperature as the best-fit using nebular abundances and a slightly higher reduced  $\chi^2$ . The most obvious difference between the best-fit models using nebular and stellar abundances is that the model with stellar abundances underestimates the emission at  $\sim 0.5$  keV due to the absence of N in the stellar chemical composition. Clearly the quality of both spectral fits are limited by the relatively small number of counts in the X-ray spectrum and it is not possible to convincingly distinguish whether the chemical composition of the X-ray emitting gas in NGC 7026 better matches that of the central star or the nebula.

From the EPIC/pn spectrum we can also determine that the volume emission measure is  $3.6^{+1.4}_{-0.8} \times 10^{55} (\frac{d}{1700 \text{ pc}})^2$  cm $^{-3}$ , where  $d$  is the distance to NGC 7026 in pc. The distance has been estimated to be

$1700^{+400}_{-200}$  pc based on the extinction to NGC 7026 (Hyung & Feibelman 2004) and on the extinction-distance relationship derived by Solf & Weinberger (1984). The observed (absorbed) X-ray flux of NGC 7026 in the 0.2–2.5 keV energy range is  $(8.8 \pm 1.2) \times 10^{-15}$  ergs cm $^{-2}$  s $^{-1}$ , and the intrinsic (unabsorbed) X-ray flux is  $(1.3^{+0.5}_{-0.4}) \times 10^{-12}$  ergs cm $^{-2}$  s $^{-1}$ . The total X-ray luminosity in the 0.2–2.5 keV energy range is  $L_{\text{X}} = (4.5^{+2.0}_{-1.6}) \times 10^{32} (\frac{d}{1700 \text{ pc}})^2$  ergs s $^{-1}$ .

### 3.3. NGC 2346

The *XMM-Newton* observations of NGC 2346 are compared with a *Hubble Space Telescope* (*HST*) WFPC2 [N II] image in Figure 3. There is no statistically significant X-ray emission associated with either the nebula or the central star in these observations. The EPIC/pn observations have been used to derive an upper limit for its X-ray luminosity using a source aperture encompassing the optical nebula. The  $3\sigma$  upper limit for the EPIC/pn count rate in the 0.3–1.25 keV band is  $4.5 \times 10^{-3}$  cnts s $^{-1}$ . To derive an upper limit of the intrinsic (unabsorbed) flux we assume a thin plasma emission model with similar temperature and nebular abundances to the one that describes the X-ray emission from NGC 7026 (see §3.2). The foreground absorption is estimated based on the observed logarithmic extinction at the H $\beta$  line,  $c(\text{H}\beta) = 0.75$  (Ciardullo et al. 1999), which corresponds to a column density of  $N_{\text{H}} = 3.0 \times 10^{21}$  cm $^{-2}$ . At a distance to NGC 2346 of 690 pc (Terzian 1993), the  $3\text{-}\sigma$  upper limit of the unabsorbed flux corresponds to an X-ray luminosity  $< 4 \times 10^{31}$  ergs s $^{-1}$ .

## 4. DISCUSSION

The *XMM-Newton* observations of NGC 7026 clearly show diffuse X-ray emission while the observations of NGC 2346 do not detect significant X-ray emission. We will now use these observations to discuss the production and evolution of hot gas in bipolar PNe.

### 4.1. NGC 7026 versus NGC 2346

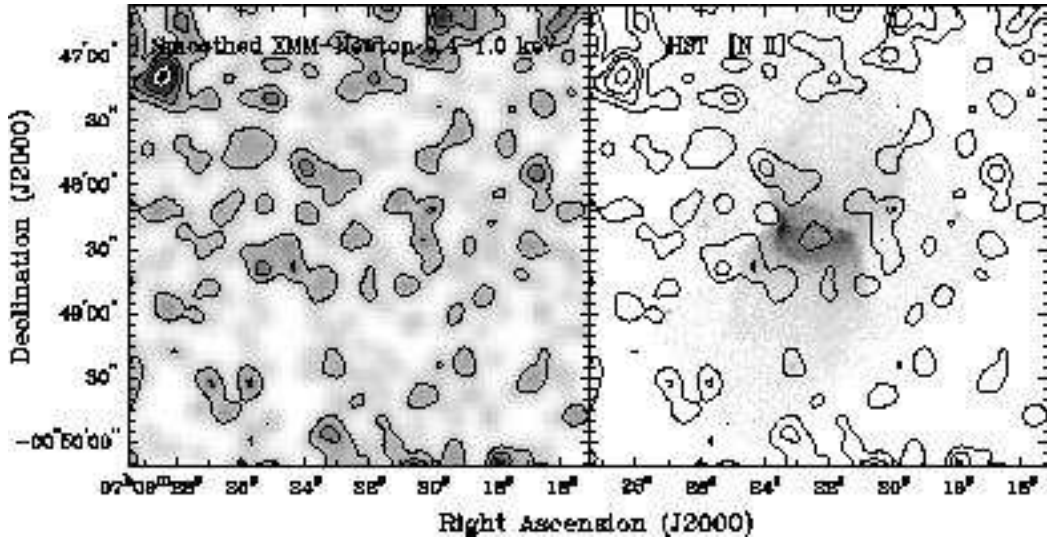


FIG. 3.— *XMM-Newton* and *HST* [N II] images of NGC 2346. (left) *XMM-Newton* EPIC image in the 0.25 – 1.5 keV band with pixel size  $2''$ . The EPIC/pn and EPIC/MOS images have been merged and the resulting image smoothed using Gaussian profiles with FWHM  $4''$  to increase the signal-to-noise ratio. The X-ray contours overlotted corresponds to the 1, 3, 5, and 9- $\sigma$  over the background. (right) *HST* WFPC2 [N II] image overlotted by the same X-ray contours.

The spatial distribution of the X-ray emission in NGC 7026 suggests that the X-ray-emitting gas is confined within the bipolar lobes, but its spatial distribution is unknown. Therefore, we define the hot gas filling factor,  $\epsilon$ , as the ratio of the emitting volume to the total nebular volume and use a reference value of 0.5 in our analysis. Using the volume emission measure determined from the spectral fits (in §3.2) and approximating the emitting volume by a  $40'' \times 15'' \times 15''$  rectangular box, the rms electron density is  $\sim 22 (d/1700\text{pc})^{-1/2} (\epsilon/0.5)^{-1/2} \text{ cm}^{-3}$ . This density and the best-fit plasma temperature can in turn be used to derive the thermal pressure of the hot gas,  $P_{\text{th}} \sim 1.9 \times n_e kT \sim 6 \times 10^{-9} (d/1700\text{pc})^{-1/2} (\epsilon/0.5)^{-1/2} \text{ dynes cm}^{-2}$ , assuming H and He are fully ionized and that the number ratio of He/H is 0.14 (the nebular abundance).

We can compare this hot gas pressure to the thermal pressure of the warm nebular shell of NGC 7026 to see whether the nebular expansion is driven by the thermal pressure as expected by the Weaver et al. (1977) model. The electron density and temperature reported by Kwitter & Henry (2001) are generally lower than those reported by Hyung & Feibelman (2004). The lowest temperature and density are derived from the [S II] lines, 6,400 K and  $3,300 \text{ cm}^{-3}$  (Kwitter & Henry 2001), resulting in a thermal pressure of  $6.3 \times 10^{-9} \text{ dynes cm}^{-2}$ . The temperatures and densities derived from a variety of lines by Hyung & Feibelman (2004) are  $\sim 9,000 \text{ K}$  and  $\sim 10^4 \text{ cm}^{-3}$ , resulting in a thermal pressure of  $\sim 2.3 \times 10^{-8} \text{ dynes cm}^{-2}$ . These measurements were made at the bright nebular waist, where the density is expected to be the highest. While the thermal pressure of the nebular gas is higher than that of the hot gas in the waist region, it is likely that the pressure of the nebular gas in the lobes is comparable to that of the hot gas.

NGC 2346 is a larger and more evolved bipolar PN than NGC 7026. No fast wind from the central star of NGC 2346 has been detected, as the *IUE* observations of the stellar C IV and N V lines do not show P Cygni

profiles (Patriarchi & Perinotto 1991). If the central star of NGC 2346 had a fast stellar wind in the past, the hot gas resulting from the shocked fast wind has either cooled or is too rarefied to be detected.

While the presence of a strong fast stellar wind is a prerequisite for the production of detectable diffuse X-ray emission, the lobe structure of bipolar PNe may also play an essential role. NGC 2346 has an open-lobe structure and lacks detectable diffuse X-ray emission and NGC 7026 has a closed-lobe structure and detectable X-ray emission. Previous X-ray observations of bipolar PNe have detected only two other nebulae, NGC 7027 and Mz 3, and both have closed-lobe structures. It is possible that open lobes allow shocked-wind to be distributed to a larger volume and the lower density precludes the detection of X-ray emission. In the case of NGC 2346, hot gas is not produced currently because of a lack of fast stellar wind. Even if it had a fast wind in the recent past, its open lobes were not able to retain the shocked stellar wind to prolong the detectability of its diffuse X-ray emission.

X-ray emission is not detected from the central star of either NGC 2346 or NGC 7026. The central star of NGC 2346 is a hot white dwarf with an A5 companion. A hot white dwarf's photospheric emission can reach the soft X-ray energy range, but is easily absorbed by the nebular gas or foreground interstellar material. A-type stars have neither fast stellar winds nor active coronae, and therefore are not expected to be X-ray sources. Even if the white dwarf possesses an accretion disk, the temperature of the accretion disk can not be high enough to produce X-ray emission. NGC 7026 has a WC-type central star. No X-ray emission has ever been detected from a single WC star even among the massive Wolf-Rayet stars (Osinkova et al. 2003) because of the high opacity in their stellar atmospheres.

#### 4.2. Hot Gas Content of Bipolar PNe

To date, only three bipolar PNe have been detected in X-rays. Among these, Mz 3 has a symbiotic central star and its X-ray emission appears to originate from interactions between its bipolar jets and the nebular material (Kastner et al. 2003). The other two, NGC 7026 and NGC 7027, are bona fide bipolar PNe. The X-ray luminosity of NGC 7026 is one of the highest among all PNe detected in X-rays. Its hot gas mass,  $\sim 0.002 \left(\frac{d}{1700\text{pc}}\right)^{5/2} (\epsilon/0.5)^{1/2} M_{\odot}$ , is also high compared to other PNe. Note however that these values may be overestimated because the X-ray-emitting lobes may have lower circum-nebular absorption than the waist region where the extinction was measured. The young bipolar PN NGC 7027 has a lower X-ray luminosity and smaller hot gas mass, but a higher hot gas temperature and density (Kastner et al. 2001). The differences between NGC 7026 and NGC 7027 might be due to an evolutionary effect, but more positive X-ray detections of bipolar PNe of intermediate ages are needed to investigate the

properties and evolution of their hot gas.

*Chandra* has observed five other bipolar PNe but none were detected. Based on these non-detections we suggest that future X-ray observations of bipolar PNe should avoid objects that have open bipolar lobes and objects with low velocity outflows ( $< 300 \text{ km s}^{-1}$ ). Instead, observations of objects with closed bipolar lobes, to confine hot gas, and with kinematic ages of no more than a few thousand years would appear best suited for understanding the generation and evolution of hot gas in bipolar PNe.

This research was supported by the NASA grant NNG04GE63G. M.A.G. acknowledges support from the grants AYA 2002-00376 and AYA 2005-01495 of the Spanish MEC (cofunded by FEDER funds) and the Spanish program Ramón y Cajal.

#### REFERENCES

- Acker, A., & Neiner, C. 2003, *A&A*, 403, 659  
 Aller, L. H. 1976, *Mem. Soc. R. Sci. Liège*, 9, 271  
 Anders, E., & Grevesse, N. 1989, *Geochimica et Cosmochimica Acta* 53, 197  
 Arias, L., Rosado, M., Salas, L., & Cruz-González, I. 2001, *AJ*, 122, 3293  
 Balucinska-Church, M., & McCammon, D. 1992, *ApJ*, 400, 699  
 Bohlin, R. C., Savage, B. D., & Drake, J. F. 1978, *ApJ*, 224, 132  
 Chu, Y.-H., Guerrero, M. A., Gruendl, R. A., Williams, R. M., & Kaler, J. B. 2001, *ApJ*, 553, L69  
 Ciardullo, R., Bond, H. E., Sipior, M. S., Fullton, L. K., Zhang, C.-Y., & Schaefer, K. G. 1999, *AJ*, 118, 488  
 Cuesta, L., Phillips, J. P., & Mampaso, A. 1996, *A&A*, 313, 243  
 Frank, A., & Mellema, G. 1994, *ApJ*, 430, 800  
 Guerrero, M. A., Chu, Y.-H., Gruendl, R. A., & Meixner, M. 2005a, *A&A*, 430, L69  
 Guerrero, M. A., Chu, Y.-H., Gruendl, R. A. 2005b, in *Planetary Nebulae as Astronomical Tools*, Eds. R. Szczerba, G. Stasinska, and S. K. Gorny, AIP Conf. Proc. 804, 157  
 Hamann, W.-R., Todt, H., & Graefener, G. 2005, in *Planetary Nebulae as Astronomical Tools*, Eds. R. Szczerba, G. Stasinska, and S. K. Gorny, AIP Conf. Proc. 804, 153  
 Hyung, S., & Feibelman, W. A. 2004, *ApJ*, 614, 745  
 Kaastra, J. S., & Mewe, R. 1993, *Legacy*, 3, 16, HEASARC, NASA  
 Kastner, J. H., Balick, B., Blackman, E. G., Frank, A., Soker, N., Vrtilek, S. D., & Li, J. 2003, *ApJ*, 591, L37  
 Kastner, J. H., Vrtilek, S. D., & Soker, N. 2001, *ApJ*, 550, L189  
 Koesterke, L. 2001, *Ap&SS*, 275, 41  
 Kwitter, K. B., & Henry, R. B. C. 2001, *ApJ*, 562, 804  
 Kwok, S. 1983, in *IAU Symposium 103, Planetary Nebulae*, ed. D. R. Flower (Dordrecht: Reidel), 293  
 Liedahl, D. A., Osterheld, A. L., & Goldstein, W. H. 1995, *ApJ*, 438, L115  
 López, J. A. 2003, *Rev. Mex. Astron. y Astrof.*, 13, 139  
 Méndez, R. H. 1978, *MNRAS*, 185, 647  
 Méndez, R. H., & Niemela, V. S. 1981, *ApJ*, 250, 240  
 Oskinova, L. M., Ignace, R., Hamann, W.-R., Pollock, A. M. T., & Brown, J. C. 2003 *A&A*, 402, 755  
 Patriarchi, P., & Perinotto, M. 1991, *A&AS*, 91, 325  
 Solf, J., & Weinberger, R. 1984, *A&A*, 130, 269  
 Su, K. Y. L., et al. 2004, *ApJS*, 154, 302  
 Terzian, Y. 1997, *IAU Symp.* 180: Planetary Nebulae, 180, 29  
 Weaver, R., McCray, R., Castor, J., Shapiro, P., & Moore, R. 1977, *ApJ*, 218, 377  
 Walsh, J. R., Meaburn, J., & Whitehead, M. J. 1991, *A&A*, 248, 613  
 Zhekov, S. A., & Perinotto, M. 1996, *A&A*, 309, 648  
 Zuckerman, B., & Gatley, I. 1988, *ApJ*, 324, 501